The influence of substitutional atoms upon the electron structure of the iron-based transition metal alloys

1998 J. Phys.: Condens. Matter 10 1825

(http://iopscience.iop.org/0953-8984/10/8/015)

J. Phys.: Condens. Matter **10** (1998) 1825–1838. Printed in the UK PII: S0953-8984(98)85201-6

The influence of substitutional atoms upon the electron structure of the iron-based transition metal alloys

B D Shanina†, V G Gavriljuk‡, A A Konchits† and S P Kolesnik†

† Institute of Semiconductor Physics, Kiev 252028, Ukraine
‡ Institute of Metal Physics, Kiev 252142, Ukraine

Received 15 June 1997, in final form 19 November 1997

Abstract. The influence of the substitutional atoms Cr, Mn, Ni, Cu, Mo in iron-based alloys on the stability of the crystalline fcc structure and the change of the electron state density at the Fermi surface are studied by means of conduction electron spin resonance (CESR). The temperature dependence of the CESR g-factor and of its integral intensity is measured and analysed in relation to theoretical predictions. It is shown that Cr, Mn and Mo decrease the state density at the Fermi surface in the fcc iron, whereas Ni and Cu increase it. The study singles out the contributions of three electron subsystems (conduction s electrons, localized isolated d electrons and those included in superparamagnetic clusters) to $g(T)$ and traces the important role of substitutional alloying elements in the formation of clusters in fcc solid solution.

1. Introduction

Face-centred-cubic iron-based alloys are used in the design of stainless austenitic steels which present a group of important engineering materials intended for severe external conditions: aggressive environment, extremely high or low temperatures etc. The crystal structure, mechanical, physical and chemical properties can be varied by changing the content of alloying elements that form substitutional solid solutions with the fcc iron. These are, mainly, Cr, Ni, Mn, Mo and others. It is clear that, ultimately, phase stability, and the mechanisms of plastic deformation and fracture are determined by the type of the interatomic bonding (see, e.g., [1]). For example, at an extremely low temperature or for rapid loading, the alloys are ductile if the metallic component of the interatomic bonding prevails and brittle if the bonding is of covalent nature. The transfer of electrons between the impurities and the host atoms occurs with a varying efficiency for s and d electrons. Atoms of the 3d group differ as to their influence on the density distribution of s and d electrons and, as a result, on the stability of the crystalline structure. A strong s–d exchange interaction in the alloys of d metals also affects the atomic ordering and the stability of the crystalline structure. On the one hand, one pays attention to magnetic transitions, magnetic structures and the formation of magnetic moments at the atoms in these alloys [2]. On the other hand, it is also important to clarify the effect of different d elements on the physical properties of the solid solution in the absence of magnetic ordering, i.e. in the paramagnetic state. From this point of view, iron-based alloys with a fcc crystalline structure are important not only as paramagnetic materials, but also as remarkable solid-state objects for studying the properties of s- and d-electron subsystems depending on the content of different substitutional atoms. We have shown in [3, 4] that the conduction electron spin-resonance (CESR) method allows one to evaluate the electron

0953-8984/98/081825+14$19.50

state density (ESD) at the Fermi surface and the correlation of s and d density components while studying the CESR temperature dependence. The integral intensity I of the CESR enables one to obtain the relative value of the ESD at the Fermi surface in theoretical analysis of the temperature dependence $I(T)$. The basic principles of such analysis are presented in [3]. The temperature dependence of the spectroscopical factor g is controlled by the following factors: (1) isolated localized spins; (2) macroscopic magnetic inclusions (superparamagnetic clusters); (3) ferromagnetic inclusions; (4) phase transitions: structural and magnetic ones. When the above contributions are small or absent, the g-factor does not depend on the temperature. In this case, the g-factor is controlled by one of the subsystems (s or d electrons) only and its value shows which subsystem is the controlling one. It is known [5–8] that the g-factor of CESR includes the contribution of d electrons due to the s–d exchange interaction. The weight factors of the s and d contributions in $g(T)$ are dependent on the magnetic susceptibilities of the corresponding electron subsystems. The spin system of d electrons in the alloy is not homogeneous. It contains isolated localized paramagnetic d states of the host and solute atoms, and macroscopic magnetic moments of the superparamagnetic clusters, if the latter occur. We have shown in [4] that the function $g(T)$ is a constant in the case of dominant s- or isolated d-electron contributions; it steadily falls or rises with an increase in temperature depending on the sign of the s–d exchange interaction when the clustering is negligible; and it emerges as a curve with a maximum when the contribution of superparamagnetic clusters with macroscopic magnetic moments is significant. In the case of ferromagnetic inclusions, the anisotropic behaviour of $g(T)$ allows the revealing of a phase transition to the ferromagnetic phase. When the external magnetic field is directed parallel (H_0) or orthogonal (H_{90}) to the sample plane, the values of the g-factor g_0 and g_{90}, respectively, are being shifted in opposite directions with a fall in temperature below the transition temperature T_C. We used the above considerations first in [4] for the separation of s and d ESD at the Fermi surface in iron-based alloys having different contents of interstitial impurities. This study seeks to clarify the effect of substitutional atoms on interatomic bonds in the iron-based fcc alloy.

2. Experimental procedure

CESR measurements are carried out across a wide temperature range from $T = 15$ K to $T = 300$ K, using an electron paramagnetic resonance spectrometer at the frequency of 9.3 GHz. We studied five sets of fcc iron-based alloys whose compositions are shown in table 1. Each set consists of samples containing one varying substitutional component as follows: Ni (samples 1, 2, 3); Cr (2, 4); Mn (2, 5, 6); Mo (2, 7, 8); Cu (4, 9).

Table 1. The chemical compositions of the alloys studied (in wt.%).

Solutes	1	2	3	4	5	6	7	8	9
Cr	15	15	15	25	15	20	15	15	25
Ni	15	20	25	20	20	20	20	20	20
Mn	—	—	—	—	5	10	—	—	—
Mo	—	—	—	—	—	—	0.6	1.3	—
Cu	—	—	—	—	—	—	—	—	2.5
Fe	70	65	60	55	60	50	64.4	63.7	52.5

The ingots, 0.5 kg in weight, were melted in the argon atmosphere using an induction furnace. The samples, of size $3.5 \times 13 \times 2 \times 10^{-2}$ mm^3, were obtained after hot forging to

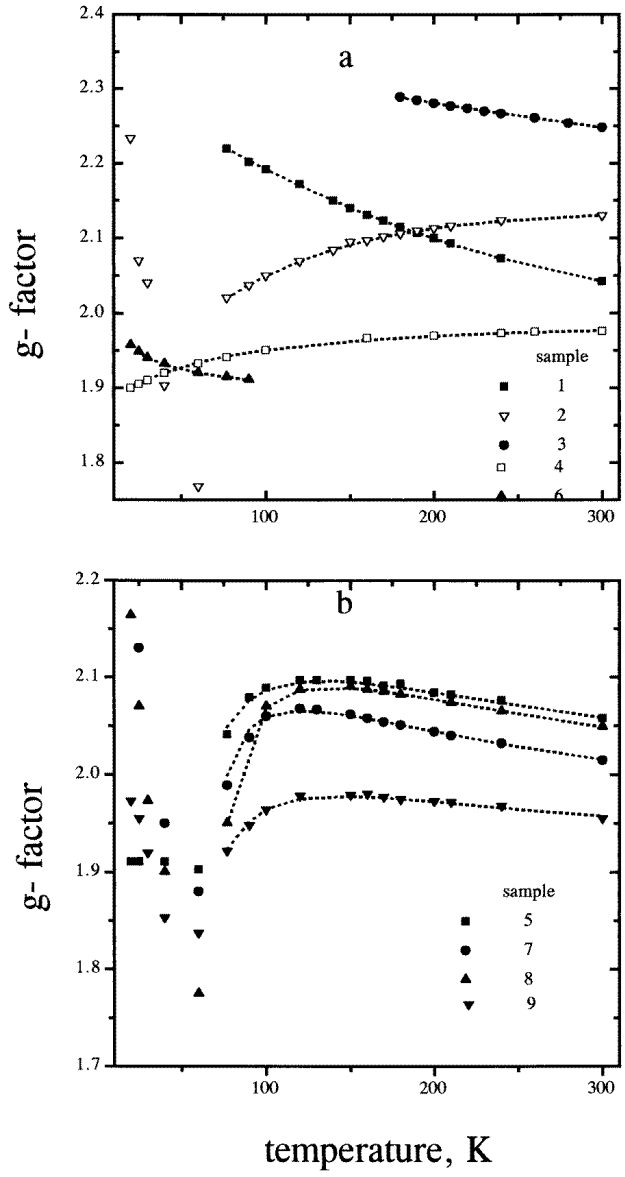

Figure 1. The temperature dependence of the CESR g-factor for samples 1–9 from table 1. Points are experimental data and lines refer to the calculated $g(T)$ for paramagnetic states; the external magnetic field H_0 lies in the sample plane.

get the rods of diameter 6 mm and cold rolling, with intermediate annealings at 1000 °C. The sample thickness $d = 2 \times 10^{-2}$ mm was sufficiently small for us to neglect the skin effect at the temperature $T > 100$ K for the alloys of the above compositions [3]. Before the measurements, the samples were solution treated in the argon atmosphere at 1100 °C, for 20 min, and this was followed by water cooling.

The CESR integral intensity is measured in units of that for a reference sample. We

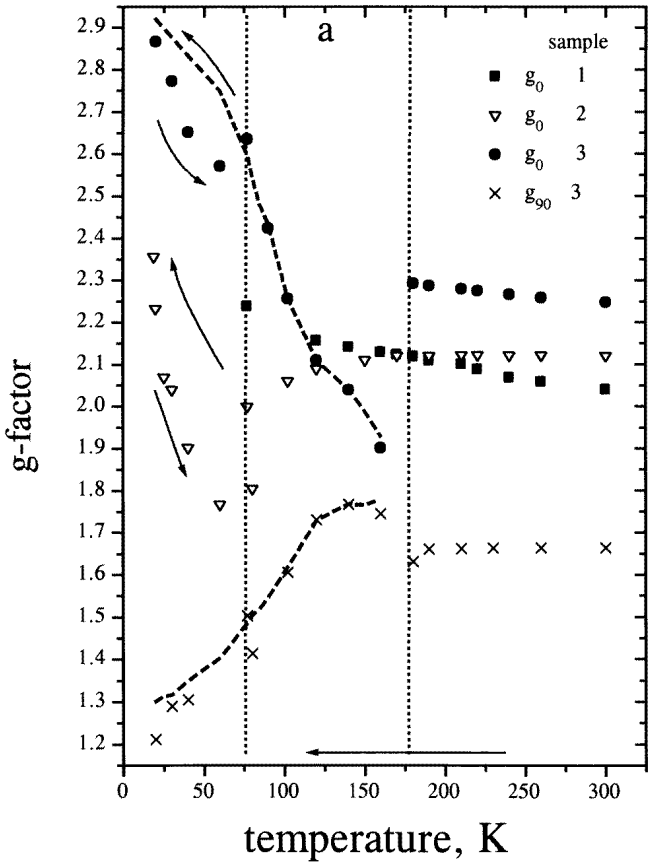

Figure 2. The temperature dependence of the g-factor (a) and the resonance signal integral intensity (b) for samples 1, 2, 3. I_0 is the integral CESR intensity for the reference sample (graphite). The dotted lines mark two phase transitions at $T_C = 175$ K and $T_g = 75$ K. Arrows show the direction of the temperature change during the measurements. The dashed lines in (a) for sample 3 are the result of the fitting of experimental data at $T < 175$ K to the formula (1).

took the sample of graphite as the reference sample, as its CESR signal and g-factor $g_C = 2.012(\pm 0.002)$ do not depend on the temperature across the actual temperature range. The graphite sample contained 10^{16} spins and was pasted over the alloy sample in the centre of the resonator cavity.

All of the measurements were carried out in two geometries: the external magnetic field H_0 lying in the sample plane ($\theta = 0^\circ$, $g = g_0$) and H_0 orthogonal to the sample plane ($\theta = 90^\circ$, $g = g_{90}$). We show $g(T)$ for just samples 3 and 9 to illustrate the ferromagnetic phase transition. In all other cases, g_0 and g_{90} have the same temperature dependence; therefore only g_0 is given.

The CESR signal was observed for all of the samples, but, in order to obtain successful measurements, it was necessary to take four of the same foils in the case of sample 1 and a third part of sample 3, because the latter produced a signal that was too powerful and overloaded the resonator cavity.

The fitting of the experimental data to theoretical expressions was performed using the computer program Peak Fit 4.

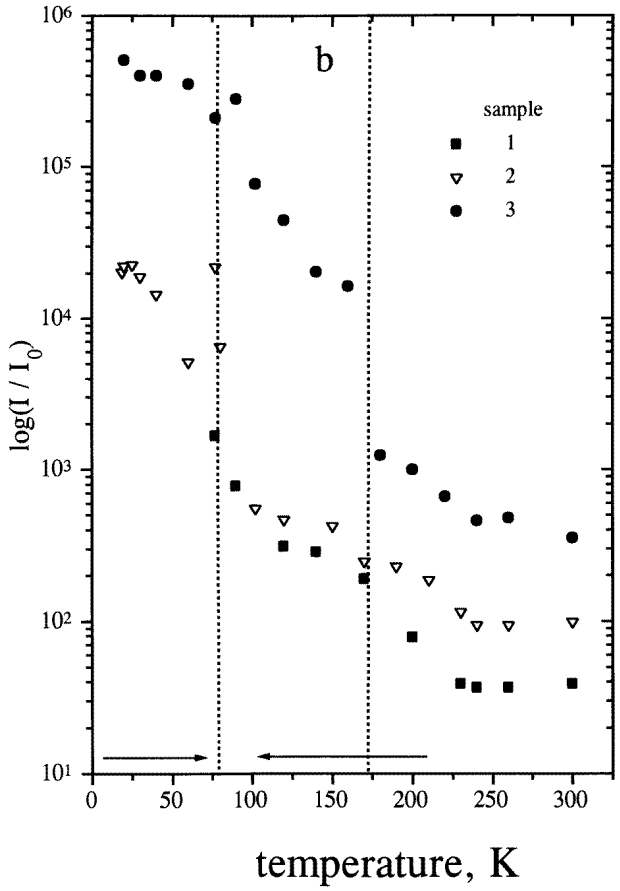

Figure 2. (Continued)

3. Results

The temperature dependence of the CESR g-factors is shown in figure 1 for all of the samples across the temperature range where the samples are in a paramagnetic state. One can see the significant change in the g-factor with the temperature, especially for samples 7, 8, 9. The values of the g-factors change over the range 1.9–2.2.

Figure 1(a) presents $g(T)$ with a simple temperature dependence looking like $1/T$ (samples 1, 3, 6) or with a weak increase of $g(T)$ as the temperature grows. Another group of samples (5, 7, 8, 9 in figure 1(b)) present $g(T)$ as a curve with a maximum. In the low-temperature range, we observe the phase transition at $T = 75$ K for all of the samples shown in figure 1(b) and for sample 2 in figure 1(a). This phase transition for most of the samples is not magnetic—as soon as their g-factors in the low-temperature range are isotropic. There are no phase transitions for samples 1, 4 and 6. In figure 1(a), we did not show $g(T)$ for sample 3 at $T < 180$ K, as will be discussed further below. Some peculiarities of the CESR behaviour are linked to the composition of the samples and the special role of substitutional elements.

Nickel. Samples 1, 2 and 3 contain different amounts of Ni: 15, 20 and 25 wt.%.

The change in the resonance signal is significant, as figure 2(b) shows. For sample 1, we observe a paramagnetic signal with a very small intensity and a weak anisotropy of the g-factor. There is no phase transition. With an increase in the nickel content, the integral intensity and anisotropy of the g-factor grow. The crystal structure becomes unsteady: at first (sample 2), the low-temperature phase transition appears at $T = 75$ K as a structural irreversible phase transition. The CESR signal remains paramagnetic. The value of the g-factor in the low-temperature phase does not return during heating to the value of the high-temperature phase at $T = 75$–80 K. In the sample with a high content of nickel (sample 3) we observe two phase transitions. The high-temperature transition at $T = 175$ K is the ferromagnetic one. As seen in figure 2(b), the intensity of the signal grows significantly to 100 times that for alloys 1 and 2 and the anisotropy of the g-factor shows ferromagnetic behaviour—g_0 and g_{90} change their values in opposite directions. The latter is connected with the anisotropy of the ferromagnetic resonance frequency (or resonance field) which is described for thin metallic samples by the following equation [9]:

$$(\omega/g_C\beta)^2 = (H_{res} + B_i \cos 2\theta)(H_{res} - B_i \sin^2\theta) \tag{1}$$

where β is Bohr magnetic moment, H is external magnetic field, $B_i = 4\pi M_s(T) - H_A$ is the magnetic induction in the sample, M_s is the spontaneous magnetization and H_A is the field of the anisotropy; g_C is the g-factor for $T \to T_C$, when B_i goes to zero; θ is the angle between $\boldsymbol{H}$ and the sample plane. In our experiments ω is the constant frequency of the microwave field. At low temperatures, $M_s(T)$ strongly increases and, according to resonance equation (1) the resonance field $H(\theta = 0)$ decreases whereas $H(\theta = 90^\circ)$ increases. In terms of the resonance g-factor which is determined as the ratio of the microwave frequency to the resonance field: $g = \omega/\beta H$, this means that g_0 grows and g_{90} goes down. This is observed in figure 2. We have performed the fitting of the experimental data for $H_{res}(T, \theta)$ for sample 3 to formula (1). As a result of the fitting, the value of the saturation magnetization $B_i = 0.23\ T$ at temperature 20 K was obtained. In the paramagnetic phase, the temperature dependence of the g-factor is weak.

Manganese. Figure 3 demonstrates the evolution of the CESR signal with the growth of the manganese content for samples 2, 5 and 6. As we noted in [4], Mn atoms lower the electron state density at the Fermi surface. Here this fact is confirmed, as seen in figure 3. As a result, we observed the electron paramagnetic resonance (EPR) of the localized Mn centres with a well split hyperfine structure (as shown in figure 3(a)). Six lines of the hyperfine structure belong to ^{55}Mn with the nuclear spin $I = 5/2$. The measured hyperfine constant $|A|$ is equal to 93.3×10^{-4} cm^{-1}, which is a typical value for Mn $^{2+}$ paramagnetic centres in most solid-state compounds with cubic symmetry of the crystalline field [10]. It is also known from the EPR measurements for the paramagnetic centre Mn^0 in semiconductors that two external s electrons change the sign of the hyperfine constant and make its value significantly smaller [11]. The value of $|A|$ observed for the metallic alloys points to the transfer of two 4s electrons of a Mn atom to empty states in the d band of Fe under the Fermi surface which are created due to the increase in the Mn content.

Figure 4 shows the temperature dependence of the g-factor for sample 5. We can see that in the low-temperature phase of sample 5 the temperature dependence of the g-factor is weak and the phase transition is spread over a wider temperature range, as compared with the case for sample 2 having the same content of Ni, Cr and 0 wt.% of Mn.

Chromium. Comparing samples 2 and 4 (figure 1(a)), which differ only in their chromium concentrations (15 wt.% and 20 wt.%, respectively), we see that the low-temperature phase transition disappears in sample 4 where the chromium content is high. Chromium decreases the CESR intensity, but to a lesser extent than Mn does.

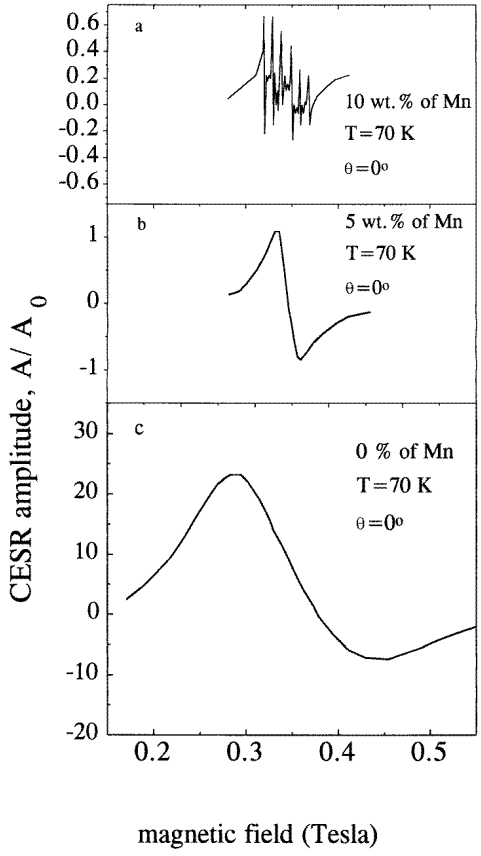

Figure 3. The change of the CESR signals for the alloys with different contents of Mn (samples 2, 5, 6). A_0 is the signal amplitude for the reference sample (graphite). (a) shows the splitting of the electron spin resonance due to the hyperfine interaction with the manganese nuclei; θ is the angle between the external magnetic field and a sample plane.

Molybdenum. Samples 7 and 8 have 0.6 wt.% and 1.3 wt.% of Mo. The effect of Mo is reduced to a change in the g-factor temperature dependence. As seen in figure 1(b), $g(T)$ for samples 7 and 8 emerges as a curve with a maximum. We showed in [4] that this kind of dependence is characteristic of $g(T)$ in the case of conduction electrons moving in a field of the superparamagnetic clusters. The higher content of Mo in the sample results in the shift of the $g(T)$ maximum to higher temperatures. The noticeable effect of Mo on $g(T)$ reflects the heterogeneous distribution of Mo atoms in the lattice. For this reason, the intensity of the CESR signal gradually decreases with the growth of the Mo content.

Copper. We compare sample 9 with 2.5 wt.% of Cu and sample 4 with the same basic composition and without Cu. Inclusion of copper results in a drastic change of $g(T)$ (figure 5). At a temperature below $T = 74$ K the sample displays the phase transition of the first kind: the g-factor does not return to its high-temperature value when the temperature changes from 16 K to 80 K. This phase transition is accompanied by a transition to the ferromagnetic state as the values of g_0 and g_{90} change in opposite directions. During the following heating, the ferromagnetism disappears at $T = 80$ K, but the crystalline structure still corresponds to the low-temperature phase, as the value of the g_0-factor is still far from

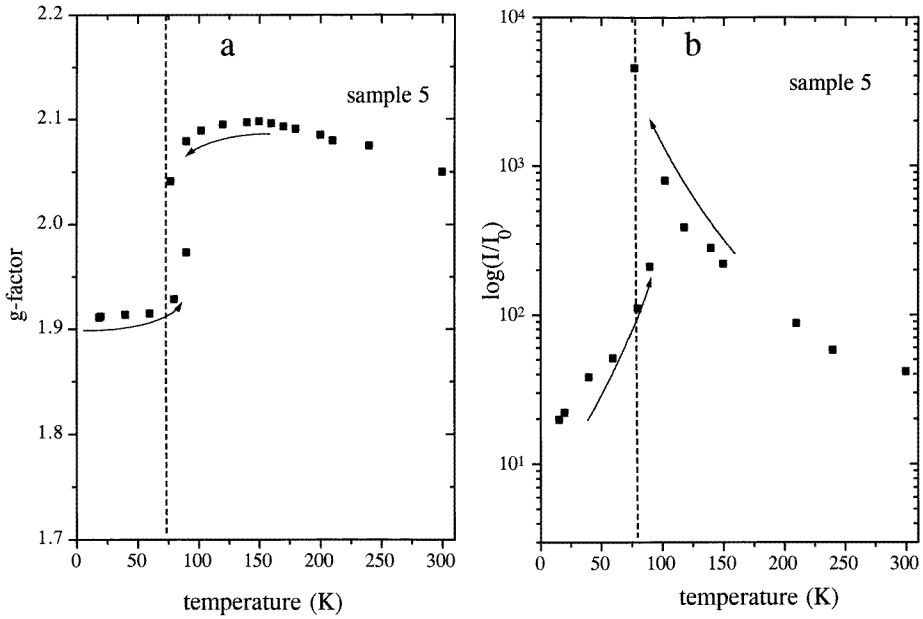

Figure 4. The low-temperature phase transition (LPT) for sample 5 containing 5 wt.% of Mn. Arrows show the direction of the temperature change during the measurements; (a) the g-factor; (b) the resonance signal intensity. Two points at $T = 80$ K and $T = 90$ K are obtained when the temperature increases from 4 K and illustrate the irreversibility of the LPT.

that in the high-temperature range measured during cooling. In the paramagnetic state, $g(T)$ contains a non-linear contribution, which points to a clustering process induced by copper.

4. Analysis

4.1. Integral intensity

Most of the samples studied enter the paramagnetic state at the temperature $T > 100$ K, except sample 3 which is paramagnetic at $T > 180$ K and samples 4 and 6 conserving the paramagnetic state to 15 K. For this reason, the analysis of the integral intensity of the CESR signal, described in detail in [3], is simplified here. The signal does not depend on the skin-layer depth δ (across a high-temperature range), which is to be expected on the basis of the small value of the CESR asymmetry parameter $R = 1.3$, a value that remains unchanged for all the samples. The line shape of the CESR signal is also the same for all of the samples provided that $\delta \geqslant d$, where d is the sample thickness. The intensities differ only in the values of the conduction electron paramagnetic susceptibility, which is proportional to the electron state density at the Fermi surface. Using the graphite sample to control the intensities, we concurrently controlled the change in the resonator quality by placing metallic foil in the resonator cavity.

The electron state density at the Fermi surface was found as

$$D(E_F) = 10^{16}(I/I_0)/V/E_F$$

where I is the CESR integral intensity of the sample studied and I_0 is the integral intensity of the graphite sample measured under the same conditions; V is the sample volume; E_F

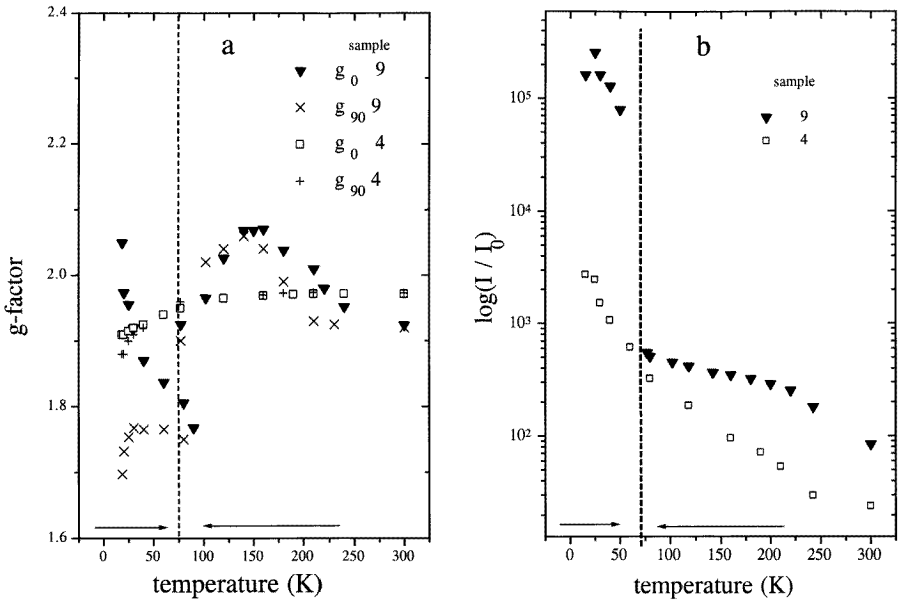

Figure 5. The temperature dependence of the g-factor (a) and the resonance signal integral intensity (b) for sample 9 containing 2.5 wt.% of Cu in comparison with sample 4 having the same content of Ni, Cr and 0 wt.% of Cu. The dotted lines mark the temperature of the phase transition. The experimental data for the orthogonal g-factors g_{90} are given for samples 4 and 9 to illustrate the ferromagnetic behaviour at $T < 75$ K. When the samples are heated from 4 K, the data for g_0 and g_{90} for sample 9 at $T > 74$ K do not coincide with those for the measurements made with temperature decreasing from 300 to 74 K, which reveals the irreversibility of the low-temperature phase transition.

Table 2. The electron state density at the Fermi surface.

Sample	1	2	3	4	5	6	7	8	9
$D(E_F)$ (10^{21} cm^{-3} eV^{-1})	0.15	0.38	1.24	0.10	0.16	0.09	0.31	0.09	0.32

is the Fermi energy of the fcc iron-based alloy, $E_F = 10.3$ eV [12]. The measurements and calculations were carried out at the temperature $T = 300$ K. The results are given in table 2.

4.2. The g-factor

The analysis of the temperature dependence of the CESR g-factors is carried out for the paramagnetic state for all the samples. The experimental data are indicated by points in figure 1. As follows from [5–8], the CESR g-factor can be written as a function of the magnetic susceptibilities of the s- and d-electron subsystems:

$$g(T) = g_s(1 + \chi_r^{-1}(T))/(g_s/g_d + \chi_r^{-1}(T)). \tag{2}$$

g_s, g_d are the g-factors of the conduction electron and of the localized d electron in the iron-based alloy in the absence of interaction between them; we found in [4] $g_s = 1.89(\pm 0.01)$

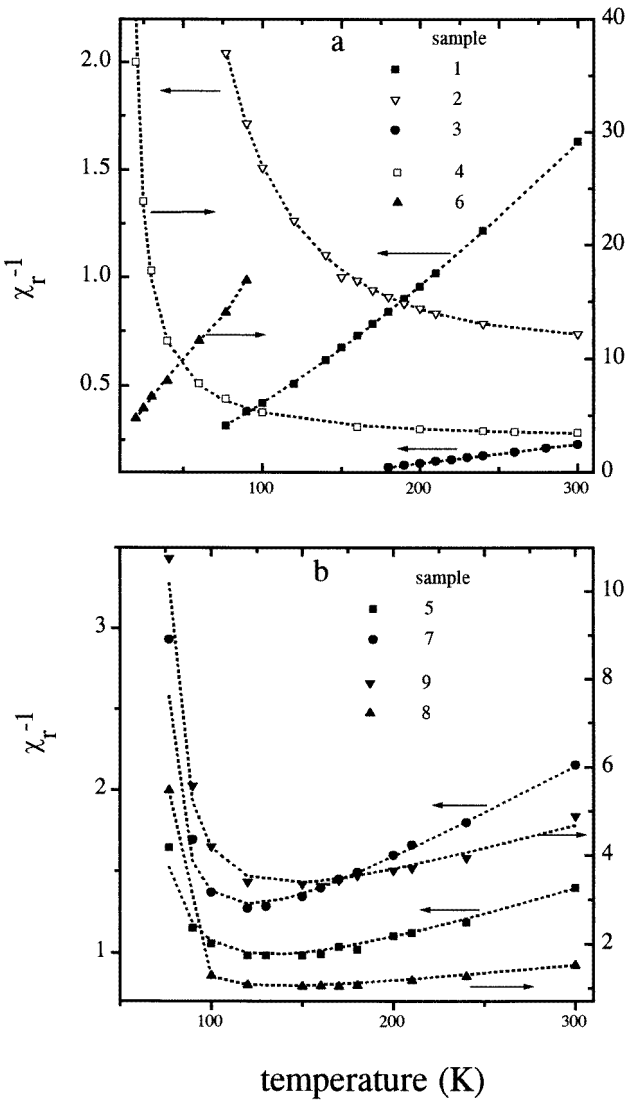

Figure 6. The temperature dependence of $\chi_r^{-1}(T) = \chi_s/\chi_d$ obtained from the experimental data in figure 1 using formula (1); the left-hand and right-hand y-axes differ only in their scales and the arrows show which axes the data are related to.

and $g_d = 2.35(\pm 0.01)$. χ_r^{-1} is the ratio of the magnetic susceptibilities of the s- and d-electron subsystems:

$$\chi_r^{-1} = \chi_s/\chi_d \tag{3}$$

$$\chi_s = \chi_{s0}(1 + \alpha_1\chi_{d0}) \qquad \chi_d = \chi_{d0}(1 + \alpha_1\chi_{s0}) \tag{4}$$

where α_1 is the parameter of the exchange interaction between the conduction electrons and the localized d electrons.

$$\chi_{s0} = 0.5g_s^2\mu_B^2 D(E_F) \tag{5}$$

is the Pauli magnetic susceptibility of the conduction electron system; χ_{d0} is the magnetic susceptibility of the isolated localized spin system which changes with the temperature according to the Curie–Weiss law:

$$\chi_{d0} = C_1/(T - \Theta_p) \tag{6}$$

where C_1 and Θ_p are the Curie constant and the paramagnetic Curie temperature. Using (2) and the experimental data for $g(T)$ from figure 1, we obtain the temperature dependence for χ_r^{-1}. It is shown in figure 6. On the other hand, as follows from relation (3) and formulae (4),

$$\chi_r^{-1}(T) = \chi_{s0}((T - \Theta_p)/C_1 + \alpha_1)/(1 + \alpha_1\chi_{s0}) \tag{7}$$

and we expect to see $\chi_r^{-1}(T)$ as a linear function of the temperature. However, figure 6 shows the strongly non-linear behaviour of $\chi_r^{-1}(T)$. We link this fact to the existence of superparamagnetic clusters in the alloys of 3d metals.

The magnetic system in an alloy is inhomogeneous and its magnetic susceptibility could be approximately described as a sum of the paramagnetic susceptibilities of two subsystems which are the localized magnetic moments of separated atoms (the d-electron spin system) and macroscopic magnetic moments M owing to superparamagnetic clusters. The magnetic cluster is a group of atoms with polarized spins as a result of interatomic interaction. The orientation of the cluster moment is arbitrary in zero magnetic field. In an external magnetic field H, the magnetic macro-moment has the energy $\overline{h}\Omega = (M/\mu_B)\mu_B H$. The value of M is proportional to the number of atoms included in the cluster. As soon as Ω is much bigger than the resonance frequency of the conduction electron, it no longer contributes to the resonance-field value. Nevertheless, the cluster contributes to the total magnetic susceptibility of the system and changes the relative sizes of the s and d contributions to the CESR resonance field.

The exchange interaction between the conduction electrons and the superparamagnetic cluster system changes the value χ_{s0} and, in the mean-field approximation, the changed χ_{s0} can be written as

$$\chi'_{s0} = \chi_{s0}/(1 - \alpha_2\chi_{d2}(T)) \tag{8}$$

where $\chi_{d2}(T)$ is the magnetic susceptibility of the superparamagnetic cluster system and obeys the Langevin law [13]:

$$\chi_{d2}(T) = C_2 L(\Theta/T) \qquad C_2 \equiv \chi_{d2}(T = 1) \tag{9}$$

$$L(\Theta/T) = \coth(\Theta/T) - T/\Theta \qquad \Theta = MH/kB. \tag{10}$$

We substitute (8) for χ_{s0} in (7) and write the temperature dependence of the $\chi_r^{-1}(T)$ as follows:

$$\chi_r^{-1}(T) = (a + bT)/(1 - c(L(\Theta/T)) \tag{11}$$

$$a = (\alpha_1(\chi_{s0} - b\Theta_p) \qquad b = \chi_{s0}/C_1 \qquad c = \alpha_2 C_2. \tag{11a}$$

In accordance with (11), in the case where $\alpha_2 > 0$ ($\alpha_2 < 0$), the expected temperature dependence displays a decay (a growth) of the χ_r^{-1} when the contribution of the clusters begins to decrease. A further rise in the temperature results in the second term in the numerator of (11) becoming dominant and in increase of the χ_r^{-1}. Therefore, there is a temperature interval where one expects non-linear behaviour with the minimum for χ_r^{-1} in the case of $\alpha_2 > 0$.

The fitting of the experimental data $g(T)$ to the theoretical expressions (2) and (11) is shown by the lines in figure 1 and figure 6. The parameters obtained, a, b, c, Θ, are given in table 3.

Table 3. Parameters of the experimental data fitted into the theory, formulae (3)–(9).

	1	2	3	4	5	6	7	8	9
a	0.082	0.257	−0.035	0.230	0.0013	1.186	−0.210	−0.089	−0.157
b (K^{-1})	0.0090	0.00056	0.0009	0.0030	0.0035	0.1760	0.0061	0.0041	0.0123
c	−1.77	1.057	0.0	1.016	1.70	—	2.84	4.5	3.25
Θ (K)	406	400	—	874	132	—	78	50.6	70

Using the $D(E_F)$ found, we obtain χ_{s0} from (4), and then, using a, b, c, Θ, find $\alpha_1 C_1$, $\alpha_2 C_2$ and C_1. To separate the contributions $\alpha_1\chi_{s0}$ and $b\Theta_p$ to the constant a in formula (11a), we supposed that the parameter α_1 of the exchange interaction between a conduction electron and localized d electrons does not depend on the concentration of substitutional solutes, whereas Θ_p which is proportional to d–d electron exchange interaction is responsible for the change in the value of a with the changing alloy composition. We have found in figure 2 that the ferromagnetic Curie temperature for sample 3 is equal to $T_C = 175$ K. The paramagnetic Curie temperature Θ_p is connected to T_C through the known equation [13] $\Theta_p = T_C(0.5z \ln[z/(z-2)])$ where $z = 12$ is the coordination number for the fcc lattice. Therefore, we evaluated $\Theta_p = 192$ K for sample 3 and then found $\alpha_1 = 0.14 \times 10^7$ from (11a), which corresponds to the antiferromagnetic exchange interaction. Supposing this value α_1 to be the same for all of the samples, we calculated $\alpha_1 C_1$ and Θ_p for other samples. The values obtained are given in table 4.

Table 4. Pauli (χ_{s0}) and Curie–Weiss (C_1) components of magnetic susceptibility of the alloy volume unit (cm^3) and the parameters of the exchange interaction energy in a mean field of localized d electrons at separated atoms ($\alpha_1 C_1$) and of superparamagnetic clusters ($\alpha_2 C_2$). K_c is the coefficient of the cluster formation.

	1	2	3	4	5	6	7	8	9
χ_{s0} (10^{-7})	0.12	0.32	1.00	0.076	0.136	0.074	0.26	0.08	0.27
C_1 (10^{-5} K^{-1})	0.133	5.716	11.36	0.253	0.385	0.0042	0.426	0.195	0.230
$\alpha_1\chi_{s0}$	0.017	0.047	0.14	0.01	0.019	0.01	0.037	0.01	0.04
$\alpha_1 C_1$ (10^2 K^{-1})	0.019	0.80	1.60	0.035	0.054	0.0006	0.06	0.027	0.032
$\alpha_2 C_2$	−1.77	1.057	0	1.016	1.70	—	2.84	4.5	3.25
Θ_p (K)	−7	−375	192	−73	5	−6.7	40	24	16
Θ (K)	406	400	—	874	132	—	78	50.6	70
K_c	378	5.3	0	254	42	—	37	84	71

The tendency towards cluster formation can be described by the parameter

$$K_c = |\alpha_2 C_2 \Theta / \alpha_1 C_1| \,. \tag{12}$$

Indeed, $\alpha_2 C_2$ is proportional to the number of clusters in the sample, Θ is proportional to the number of atoms in the cluster, and their product is proportional to the number of d electrons included in the cluster system. On the other hand, $\alpha_1 C_1$ is proportional to the number of localized d electrons owing to the separated atoms. Therefore, K_c describes the ratio of the value of the interaction energy of conduction electrons in a mean field of the cluster system to that in a mean field of the system of isolated localized d electrons. When K_c is large, the solid solution has a tendency to form clusters. The last row in table 4 contains the calculated values of K_c.

5. Discussion

CESR measurements and the analysis of the temperature dependence of the integral intensity and g-factors of CESR allow us to obtain the change of the s and d ESD at the Fermi surface depending on the alloy composition. The values of the magnetic susceptibilities χ_{s0} and C_1, as given in table 4, show that the ESD of the conduction electrons increases with the growth of the Ni and Cu content and decreases with higher concentrations of Cr, Mn and Mo. The ESD of d electrons at the Fermi surface grows only in the case of higher nickel concentrations.

The exchange interaction between s electrons and isolated localized d electrons is antiferromagnetic ($\alpha_1 > 0$). The exchange interaction of the conduction electrons with the clusters is also antiferromagnetic ($\alpha_2 > 0$) except for sample 1.

The stability of the solid solution becomes lower due to cluster formation. Clusters exist in all of the samples, except sample 3, but their relative contributions are different. The curves in figure 1(b) show that the contribution of clusters is visible for the alloys with Mn (sample 5), Mo (samples 7, 8) and Cu (sample 9). The empirical factor K_c linked to the ferromagnetic exchange interaction between conduction electrons and the cluster system grows also in the case of Mo (compare samples 7, 8 with sample 2), Mn (compare samples 5 and 2) and decreases in the case of Cu (compare 9 and 4). The cluster formation induced by the presence of Cr is efficiently suppressed under the influence of nickel. Nickel causes an increase in the s-electron-state density and in the metallic component of the interatomic bonding. At the same time, the increase of the d-electron-state density results in the phase transition to the ferromagnetic state (sample 3) at $T_C = 175$ K.

Manganese brings down the ESD at the Fermi surface of the iron-based alloy drastically as compared to other substitutional impurities. The value of the hyperfine EPR splitting provides evidence for the transfer of two s electrons of Mn into the d band of Fe, which reflects the enhanced covalent bonding.

The low-temperature phase transition (LPT) of the first kind, observed in samples 2, 3, 5, 7–9 at $T = 75(\pm 2)$ K is not complete, as we can see in sample 3 (figure 2(a)) where a small contribution of the (LPT) phase in $g(T)$ is observed along with the ferromagnetic behaviour of the g-factor in the fcc phase. Manganese (see figure 4 for sample 5) causes a wide temperature hysteresis of this phase transition (ΔT, between the direct and inverse transitions). Chromium suppresses the LPT when its concentration is higher than the nickel concentration. The LPT observed here is a well known transition from fcc γ-phase to hcp ε-phase. It takes place in Fe–Cr–Ni and Fe–Mn alloys (see, e.g., [14, 15]). This phase transition is due to the splitting of dislocations in (111) planes and it occurs in the iron-based alloys having low values of the stacking fault energy (SFE). That is why the decrease in the value of SFE promotes this transition. The above-described effects of chromium, nickel and manganese on the appearance of the ε-phase in fcc iron-based alloys at low temperatures depend on the combined influence of the elements on the value of the SFE and its temperature dependence, both of these being affected by the state density at the Fermi surface.

6. Conclusions

We have separated the contributions of localized and conduction electron subsystems to the g-factor of the CESR signal and have shown that the non-linear behaviour of the magnetic susceptibility is explained by the formation of superparamagnetic clusters due to inhomogeneous distribution of substitutional solutes. The alloying with Ni and Cu results in

increase of the conduction electron density (ESD) at the Fermi surface, whereas additions of Cr, Mn and Mo decrease it. The cluster formation is enhanced in the case of high concentrations of Cr, Mo and Mn. We revealed a low-temperature phase transition of the first kind in all of the samples except the sample with a higher concentration of Cr as compared to its Ni concentration. The alloying with Cu and Ni results in coexistence of the low-temperature phase and ferromagnetism.

Acknowledgments

This study was performed within the framework of the project BMBF-03 N 900020, Germany. The authors are deeply grateful to Professor Dr Ing H Berns for support of this study and useful discussion.

References

[1] Morinaga M, Yukawa N and Ezaki H 1985 *Phil. Mag.* A **51** 223
[2] Matsumoto Y, Morinaga M, Namba T and Sakaki T 1996 *J. Phys.: Condens. Matter* **8** 3619
[3] Gavriljuk V G, Efimenko S P, Smuk Ye E, Smuk S U, Shanina B D, Baran N P and Maksimenko V M 1993 *Phys. Rev.* B **46** 3224
[4] Shanina B D, Gavriljuk V G, Konchits A A, Kolesnik S P and Tarasenko A V 1995 *Phys. Status Solidi* a **149** 711
[5] Hasegawa H 1959 *Progr. Theor. Phys. (Kyoto)* **21** 483
[6] Schultz S, Schanaberger M R and Platzman P M 1967 *Phys. Rev. Lett.* **19** 749
[7] Pifer J H and Longo R T 1971 *Phys. Rev.* B **4** 3797
[8] Pifer J H and Magno R 1971 *Phys. Rev.* B **3** 663
[9] Smith J and Beljers H C 1955 *Philips Res. Rep.* **10** 113
[10] Abragam A and Bleaney B 1970 *Electron Paramagnetic Resonance of Transition Ions* vol 1 (Oxford: Clarendon)
[11] Ludwig G W and Woodbury H H 1959 *Phys. Rev.* **113** 1014
[12] Wood J H 1962 *Phys. Rev.* **126** 517
[13] Vonsovskij S V 1971 *Magnetism* (Moskow: Nauka)
[14] Schumann H 1969 *Arch. Eisenhüttenwes.* **40** 1047
[15] Fujita H and Katayama T 1992 *Mater. Trans. Japan Inst. Met.* **33** 243